Nanocluster Formation Synthetic, Kinetic, and Mechanistic Studies.† The Detection of, and Then Methods To Avoid, Hydrogen Mass-Transfer Limitations in the Synthesis of Polyoxoanion- and Tetrabutylammonium-Stabilized, Near-Monodisperse 40 ± 6 Å Rh(0) Nanoclusters

John D. Aiken III and Richard G. Finke*

Contribution from the Department of Chemistry, Colorado State University, Fort Collins, Colorado 80523

Received June 12, 1997. Revised Manuscript Received July 17, 1998

Abstract: Previously we reported $P_2W_{15}Nb_3O_{62}^{9-}$ polyoxoanion- and Bu_4N^+-stabilized, 20 ± 3 Å, $Ir(0)_{\sim 300}$ nanoclusters. These nanoscopic materials are synthesized from the reduction of $[(C_4H_9)_4N]_5Na_3[(1,5\text{-COD})M{\cdot}P_2W_{15}Nb_3O_{62}]$ (M = Ir) by H_2 in acetone and are isolable, highly catalytically active, with an unprecedented catalytic lifetime in solution. However, an initial attempt to synthesize Rh(0) nanoclusters from the analogous M = Rh precursor, and under conditions otherwise identical to the M = Ir synthesis, led to polydisperse 16 to 116 Å Rh(0) nanoclusters. The above results led, in turn, to the discovery that H_2 gas-to-solution mass-transfer limitations (MTL) were responsible for the failure of the initial synthesis, an important finding since H_2 is one of the most common reducing agents in syntheses of modern, near-monodisperse transition metal nanoclusters. The finding of a hydrogen MTL regime is fortified by stirring-rate-dependence data, kinetic data [demonstrating a catalyst nondependent (MTL) regime, and a catalyst-dependent (chemical-reaction rate-limiting) regime], and transmission electron microscopy used as a mechanistic probe. The results provided evidence for a growth mechanism involving parallel autocatalytic surface growth (leading to near-monodisperse nanoclusters) in competition with diffusive agglomeration (leading to polydisperse nanoclusters). The above mechanistic insights were then used, in turn, to design conditions where only the autocatalytic surface-growth pathway occurs, conditions which led to the successful synthesis of the desired near-monodisperse, 40 ± 6 Å Rh(0) $P_2W_{15}Nb_3O_{62}^{9-}$ polyoxoanion- and Bu_4N^+-stabilized nanoclusters. The resultant Rh(0) nanoclusters are only the second example of polyoxoanion- and Bu_4N^+-stabilized transition metal nanoclusters.

Introduction

Presently there is considerable interest in the synthesis of *near-monodisperse* (≤±15% in diameter) nanoclusters[1] (<10 nm or 100 Å).[2] In particular there is interest in controlling the size, size-distribution, composition, and shape of such clusters via designed syntheses. However, and despite the fact that metal colloids (>10 nm or 100 Å) have been known for over 140 years,[3] general methods for the designed synthesis of a prechosen transition metal nanocluster remain unavailable—a statement that is still true despite some notable recent synthetic advances.[4] In fact, the empiricism in existing nanocluster synthetic routes

† Part IV in a series.

(1) Reviews on nanoclusters: (a) Jena, P.; Rao B. K.; Khanna, S. N. *Physics and Chemistry of Small Clusters*; Plenum: New York, 1987. (b) Andres, R. P.; Averback, R. S.; Brown, W. L.; Brus, L. E.; Goddard, W. A.; Kaldor, A.; Louie S. G.; Moscovits, M.; Peercy, P. S.; Riley, S. J.; Siegel, R. W.; Spaepen, F.; Wang, Y. *J. Mater. Res.* **1989**, *4*, 704. This is a Panel Report from the United States Department of Energy, Council on Materials Science on "Research Opportunities on Clusters and Cluster-assembled Materials". (c) Thomas, J. M. *Pure Appl. Chem.* **1988**, *60*, 1517. (d) Henglein, A. *Chem. Rev.* **1989**, *89*, 1861. (e) A superb series of papers, complete with a record of the insightful comments by the experts attending the conference, is available in: *Faraday Discuss.* **1991**, *92*, 1−300. (f) Bradley, J. S. In *Clusters and Colloids. From Theory to Applications*; Schmid, G., Ed.; VCH: New York, 1994; pp 459−544. (g) Schmid, G. In *Aspects of Homogeneous Catalysis*; Ugo, R., Ed.; Kluwer: Dordrecht, 1990; Chapter 1. (h) Bönnemann, H.; Braun, G.; Brijoux, W.; Brinkmann, R.; Tilling, A. S.; Seevogel, K.; Siepen, K. *J. Organomet. Chem.* **1996**, *520*, 143−162 and the collection of "key publications" cited as refs 2−61 therein. (i) *Active Metals: Preparation, Characterization, Applications*; Fürstner, A., Ed.; VCH: Weinheim, 1996. (j) Schmid, G. in *Applied Homogeneous Catalysis with Organometallic Compounds*; Cornils, B., Herrmann, W. A., Eds.; VCH: Weinheim, 1996; Vol. 2.

(2) (a) See elsewhere for a review of nanocluster catalysis, which includes necessary key terms and definitions of:[2b] nanoclusters; traditional colloids; monodisperse and near-monodisperse nanoparticles; "magic number" (i.e., full shell and thus enhanced stability) nanoclusters; Schwartz's updated definition of homogeneous vs heterogeneous catalysts; and inorganic ("charge") and organic ("steric") stabilization mechanisms for colloids and nanoparticles. A review of the Bu_4N^+ and polyoxoanion-stabilized $Ir(0)_{\sim 300}$ nanoclusters is also provided in that review.[2b] (b) Aiken, J. D., III; Lin, Y.; Finke, R. G. *J. Mol. Catal.* **1996**, *114*, 29−51.

(3) Faraday, M. *Philos. Trans. R. Soc.* **1857**, *147*, 145.

(4) (a) For instance, see Professor Reetz's important electrochemical synthesis[4c] (see elsewhere for a discussion of this interesting method),[2b] as well as the papers cited in refs 15−19 of ref 8a. (b) Reetz, M. T.; Helbig, W.; Quaiser, S. A.; Stimming, U.; Breuer, N.; Vogel, R. *Science* **1995**, *267*, 367. (c) Reetz, M. T.; Helbig, W. *J. Am. Chem. Soc.* **1994**, *116*, 7401. (d) Reetz, M. T.; Quaiser, S. A. *Angew. Chem., Int. Eng. Ed.* **1995**, *34*, 2240. (e) Reetz, M. T.; Helbig, W.; Quaiser, S. A. *Chem. Mater.* **1995**, *7*, 2227. (f) Reetz, M. T.; Quaiser, S. A.; Breinbauer, R.; Tesche, B. *Angew. Chem., Int. Eng. Ed.* **1995**, *34*, 2728. (g) Reetz, M. T.; Lohmer, G. *Chem. Commun.* **1996**, 1921. (h) Reetz, M. T.; Breinbauer, R.; Wanninger, K. *Tetrahedron Lett.* **1996**, *37*, 4499. (i) Review: Reetz, M. T.; Helbig, W.; Quaiser, S. A. In *Active Metals*; Fürstner, A., Ed.; VCH Publishers: New York, 1996; Chapter 7, pp 279−297. (j) Kolb, U.; Quaiser, S. A.; Winter, M. A.; Reetz, M. T. *Chem. Mater.* **1996**, *8*, 1889.

S0002-7863(97)01948-3 CCC: $15.00
Published on Web 09/02/1998

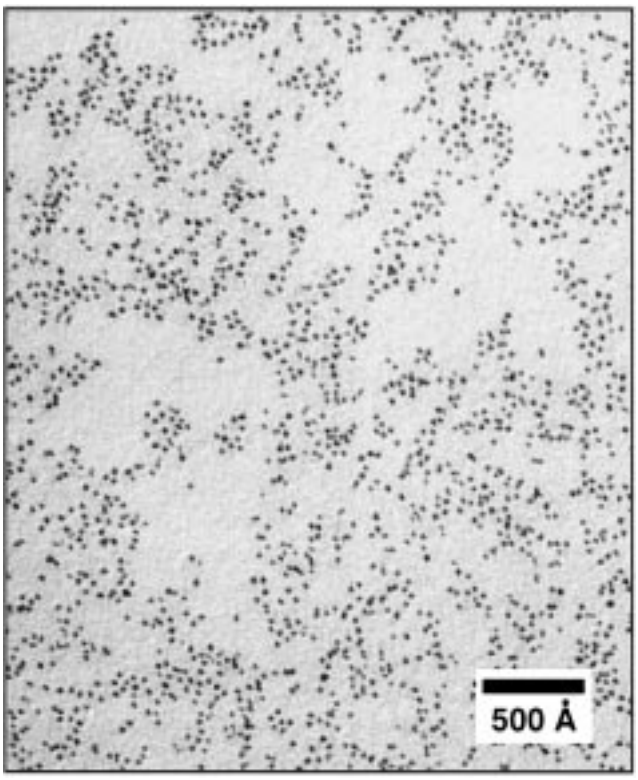

Figure 1. TEM image (100K magnification) of near-monodisperse $Ir(0)_{\sim 300}$ nanoclusters grown by the reduction of 1.2 mM **1** in acetone under chemical-reaction-rate-limiting (i.e., *non*-MTL) conditions. This image shows $Ir(0)_{\sim 300}$ nanoclusters that are 20 ± 3 Å (i.e., ±15%) in diameter.

has led to comments in the literature expressing frustration over the lack of clear, generally applicable synthetic guidelines and mechanistic insights.[1f,g,5]

Previously we reported the synthesis of near-monodispersed, polyoxoanion- and tetrabutylammonium-stabilized, 20 ± 3 Å $Ir(0)_{\sim 300}$ nanoclusters,[6] Figure 1. That synthesis is based on our polyoxoanion-supported[7] organometallic precursor $[(n\text{-}C_4H_9)_4N]_5Na_3[(1,5\text{-COD})Ir{\cdot}P_2W_{15}Nb_3O_{62}]$, **1**, and involves reducing this complex under hydrogen in acetone and in the presence of cyclohexene as a catalytic substrate (vide infra), eq

(5) (a) Weller, H. *Angew Chem., Int. Ed. Engl.* **1993**, *32*, 41−53. (b) Matijevic, E. *Chem. Mater.* **1993**, *5*, 412. (c) Steigerwald, M. L.; Brus, L. *Acc. Chem. Res.* **1990**, *23*, 183. (d) Beattie, J. K. *Pure Appl. Chem.* **1989**, *61*, 937. (e) See also the quotes and references provided in footnotes 5 and 7 elsewhere.[8a] (f) LaMer's classic work on the mechanism of formation of sulfur sols involving (i) "burst" nucleation from supersaturated solution, and (ii) diffusive growth: LaMer, V. K.; Dinegar, R. H. *J. Am. Chem. Soc.* **1950**, *72*, 4847. Lamer, V. K. *Ind. Eng. Chem.* **1952**, *44*, 1270.

(6) (a) Lin, Y.; Finke, R. G. *J. Am. Chem. Soc.* **1994**, *116*, 8335−8353. (b) As described in refs 29 and 43a of ref 6a, we *represent* the 20 ± 3 Å distribution of $Ir(0)_{\sim 190}$ to $Ir(0)_{\sim 450}$ nanoclusters present as their *average* composition of $Ir(0)_{\sim 300}$ for convenience and clarity, *only*. We *do not* mean to imply that a perfectly monodispersed, exactly $Ir(0)_{\sim 300}$, cluster is the only particle present. Similarly, we use $Ir(0)_{\sim 900}$ to represent 30 ± 4 Å $Ir(0)_{\sim 640}$ to $Ir(0)_{\sim 1460}$ nanoclusters. (c) Note that it is important to avoid the misunderstanding possible from the use, in the literature, of "Pd_{561}" to represent what is really $Pd_{570\pm 30}(phen)_{63\pm 3}(OAc)_{190\pm 10}]^{x-}$,[6d] or "$Au_{55}(PPh_3)_{12}Cl_6$" to represent what is now realized to be "$Au_{67}(PPh_3)_{14}Cl_8$ with small clusters as impurities".[6e] (d) Vargaftik, M. N.; Zagorodnikov, V. P.; Stolarov, I. P.; Moiseev, I. I.; Kockubey, D. I.; Likholobov, V. A.; Chuvilin, A. L.; Zamaraev, K. I. *J. Mol. Catal.* **1989**, *53*, 315. (e) Fackler, J. P.; McNeil, C. J.; Winpenny, R. E. P.; Pignolet, L. H. *J. Am. Chem. Soc.* **1989**, *111*, 6434−6435.

(7) $P_2W_{15}Nb_3O_{62}^{9-}$ synthesis and characterization papers: (a) Weiner, H.; Aiken, J. D., III; Finke, R. G. *Inorg. Chem.* **1996**, *34*, 7905 and references therein. (b) Finke, R. G.; Lyon, D. K.; Nomiya, K.; Weakley, T. J. *Acta Crystallogr., Sec. C* **1990**, *46*, 1592. (c) Edlund, D. J.; Saxton, R. J.; Lyon, D. K.; Finke, R. G. *Organometallics* **1988**, *7*, 1692.

Scheme 1. The Minimum Mechanism Uncovered Previously[8a] for the Formation of Ir(0) Nanoclusters[a]

A. Nucleation (slow, continuous and homogeneous)

$$\mathbf{A} \xrightarrow{k_1} \mathbf{B}$$

$$(1,5\text{-COD})Ir{\bullet}P_2W_{15}Nb_3O_{62}^{8-} + x\ \text{acetone} \underset{}{\overset{K_{eq} << 1}{\rightleftharpoons}} Ir(1,5\text{-COD})(\text{acetone})_x^{+} + P_2W_{15}Nb_3O_{62}^{9-} \quad (I)$$

$$Ir(1,5\text{-COD})(\text{acetone})_x^{+} + 2.5\ H_2 \longrightarrow \bigcirc + Ir(0) + H^{+} \quad (II)$$

$$n\ Ir(0) \xrightarrow{\textit{Homogeneous Nucleation}} [Ir(0)]_n \quad (III)$$

B. Autocatalytic Surface Growth (fast)

$$\mathbf{A} + \mathbf{B} \xrightarrow{k_2} \mathbf{2B}$$

$$(1,5\text{-COD})Ir{\bullet}P_2W_{15}Nb_3O_{62}^{8-} + 2.5\ H_2 + [Ir(0)]_n \xrightarrow{\textit{Autocatalysis}} Ir[(0)]_{n+1} + H^{+} + P_2W_{15}Nb_3O_{62}^{9-} + \bigcirc \quad (IV)$$

C. Diffusive, Agglomerative Growth

$$[Ir(0)]_n + [Ir(0)]_m \xrightarrow[\textit{Agglomeration}]{\textit{Diffusive}} [Ir(0)]_{n+m} \quad (V)$$

[a] This mechanism consists of (a) slow, continuous, homogeneous nucleation (steps I−III), rate constant k_1 for the pseudo-elementary step[8a] A → B, followed by (b) fast, autocatalytic surface growth (step IV), rate constant k_2 for the pseudo-elementary step[8a] A + B → 2B. Nucleation and growth are *separated in time* since $k_1 \ll k_2[B]$, which in turn is a key to the observed formation of a near-monodisperse (≤±15%) particle size distribution. In this example, diffusive agglomeration (step V) does not compete kinetically with autocatalytic surface growth, although literature precedent suggests that this step always occurs at a finite rate.[18]

1. The nanocluster formation reaction can be followed directly by monitoring the production of cyclooctane throughout the course of the reaction.

$$300[(1,5\text{-COD})Ir{\bullet}P_2W_{15}Nb_3O_{62}]^{8-} + 750H_2 \longrightarrow$$
$$300\ \bigcirc + 1Ir(0)_{\sim 300}{\bullet}(P_2W_{15}Nb_3O_{62}^{9-})_{\sim 66} + \sim 234[P_2W_{15}Nb_3O_{62}]^{9-} + 300H^{+} \quad (1)$$

We have studied the kinetics and mechanism of this reaction in detail for the iridium example; the results led to the finding that nanocluster growth occurs by a non-LaMer mechanism[5f] involving a sequence of (i) slow, continuous nucleation and (ii) *autocatalytic surface growth*, Scheme 1.[8] Significant features of this new mechanism are that it predicts the formation of near-

(8) (a) Part I: Watzky, M. A.; Finke, R. G. *J. Am. Chem. Soc.* **1997**, *119*, 10382−10400. (b) Part II: Watzky, M. A.; Finke, R. G. *Chem. Mater.* **1997**, *9*, 3083−3095. (c) Part III: Transition Metal Nanocluster Formation Kinetics and Mechanism. A New Kinetic Method Based on Catalytic Activity and the Concept of Pseudoelementary Steps. Watzky, M. A.; Widegren, J. A.; Aiken, J. D., III; Finke, R. G. Submitted for publication.

monodisperse nanoclusters, and that it can rationalize the formation of so-called "magic number" clusters.[8b] Additional synthetic insights and testable mechanistic predictions are available[8b] based on the realization that nanocluster autocatalytic surface growth is a "living (metal) polymer" phenomenon.[8b] The rate constants k_1 and k_2, Scheme 1, can be determined from curve fitting the H_2 pressure vs time to the appropriate analytic kinetic equations. The rate constant k_1 measures the overall nucleation process while the k_2 measures nanocluster growth.[8a]

Herein we report our discovery of, and subsequent mechanistic data fortifying, an important guideline in nanocluster syntheses: the need to *avoid hydrogen-mass-transfer limitations* when synthesizing near-monodisperse transition metal nanoclusters under H_2, especially when using rhodium and other, more catalytically active second row metals. This finding was discovered during our initial attempts to synthesize near-monodisperse rhodium nanoclusters by the route we previously synthesized polyoxoanion-stabilized $Ir(0)_{\sim 300}$ nanoclusters.[6,9] By using several "fingerprint" tests from the well-established mass-transfer literature, we show herein that nanoclusters grown under hydrogen mass-transfer-limiting (MTL) conditions are polydisperse and irregularly shaped in comparison to the near-monodisperse, spherical 40 ± 6 Å Rh(0) nanoclusters grown under non-mass-transfer-limiting (non-MTL), chemical-reaction-rate-limiting conditions. The results reveal the dramatic effects on nanocluster shape and dispersity (see Figures 1−4) and show that the solution hydrogen concentration provides one simple but crucial parameter in the synthesis of near-monodisperse, ≤15% size distribution, transition metal nanoclusters. The present study is a continuation of our kinetic, mechanistic, and synthetic studies into nanocluster formation reactions.[8]

Results and Discussion

Transmission Electron Microscopy (TEM) Studies. Distinguishing between Polydisperse (≫15% Size Distribution) and Near-Monodisperse (≤15% Size Distribution) Transition Metal Nanoclusters. The easiest way to illustrate the dramatic effects observed by running nanocluster syntheses under hydrogen mass-transfer-limited, vs chemical-reaction-rate-limited, conditions is to view Figures 1−4. Figure 1 shows the spherical, near-monodisperse, 20 ± 3 Å $Ir(0)_{\sim 300}$ nanoclusters obtained beginning from the Ir(I) precursor **1** under our previously developed Standard Conditions[6a] (40 psig H_2, 22 °C and 1.2 ± 0.1 mM **1**). Figure 2 shows *dramatically different*, irregularly shaped, polydisperse-sized, 16 to 116 Å $Rh_{\sim 520}$ to $Rh_{\sim 60000}$ nanoclusters obtained when we applied the identical conditions to the rhodium precatalyst, **2**. Note that the *only* difference between the syntheses used for the results shown in Figure 1 vs Figure 2 is the iridium vs rhodium metal in the precursor: $[(1,5\text{-COD})Ir{\cdot}P_2W_{15}Nb_3O_{62}]^{8-}$ (**1**), or $[(1,5\text{-COD})Rh{\cdot}P_2W_{15}Nb_3O_{62}]^{8-}$ (**2**).

Having seen preliminary evidence for cluster agglomeration in our earlier work,[10] and noting that rhodium nanoclusters were much more active cyclohexene hydrogenation catalysts than their iridium counterparts, we postulated that the polydisperse rhodium clusters shown in Figure 2 are the result of hydrogen gas-to-solution, MTL reaction conditions. Furthermore, we realized that this observation was an important one, given that hydrogen is one of the most widely used reductants in transition metal nanocluster syntheses in the literature,[11] and given that size control and narrow particle size distributions are key, current research goals in nanocluster science.[5] Hence, to test this hypothesis, and to attempt to grow *near-monodisperse* rhodium nanoclusters, we altered the synthetic reaction conditions in a

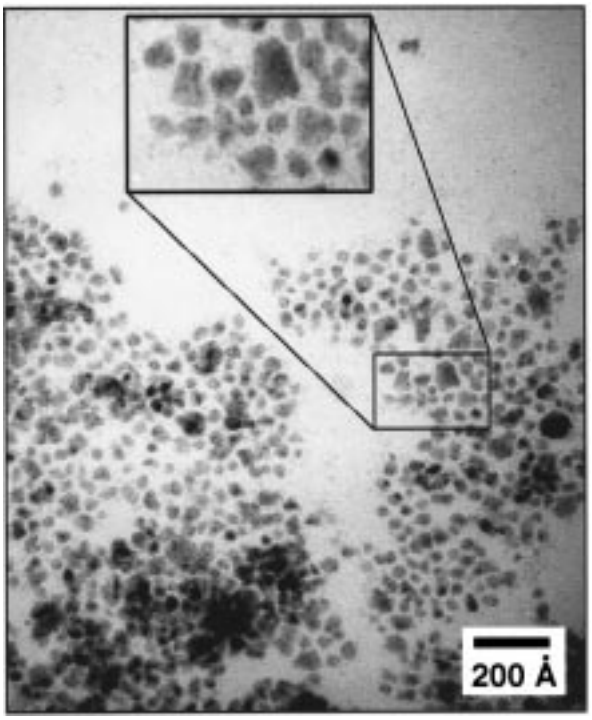

Figure 2. TEM image (430K magnification) of polydisperse rhodium nanoclusters grown by the reduction of 1.2 mM **2** in acetone under *hydrogen mass-transfer-limiting* conditions and isolated following 100% conversion of the precursor. The clusters have irregular shapes (see the inset) and range in size from 16 to 116 Å with an average diameter of 40 ± 14 Å (i.e., ± 35%). A particle size histogram of this sample is provided as Figure C of the Supporting Information.

(9) Lin, Y.; Finke, R. G. *Inorg. Chem.* **1994**, *33*, 4891−4910.

(10) (a) There are but two other systems that provide some initial hints, and thus some precedent, for the hydrogen MTL effects seen herein. One is our own initial study of nanoclusters syntheses, in particular Step V in the mechanistic scheme in Figure 13 on pp 8346−8347 elsewhere.[6a] The second is Whitesides' work studying the reactions and stereochemistry of Pt metal surface alkyls with H_2 or D_2. Note, however, that the metal products were not a focus, and thus were not studied, in Whitesides' series of valuable papers.[b−f] (b) Lee, T. R.; Whitesides, G. M. *Acc. Chem. Res.* **1992**, *25*, 266−272. (c) Lee, T. R.; Whitesides, G. M. *J. Am. Chem. Soc.* **1991**, *113*, 2568−2576. (d) Lee, T. R.; Whitesides, G. M. *J. Am. Chem. Soc.* **1991**, *113*, 368−369. (e) Lee, T. R.; Laibinis, P. E.; Folkers, J. P.; Whitesides, G. M. *Pure Appl. Chem.* **1991**, *63*, 821−828. (f) Miller, T. M.; Whitesides, G. M. *J. Am. Chem. Soc.* **1988**, *110*, 3164−3170.

(11) Some examples of nanoparticles grown with hydrogen as a reducing agent include: (a) Yonezawa, T.; Tominaga, T.; Richard, D. *J. Chem. Soc., Dalton Trans.* **1996**, 783. (b) A review: Bönnemann, H.; Brijoux, W. In *Active Metals: Preparation, Characterization, Applications*; Füstner, A., Ed.; VCH: Weinheim, 1996. See especially p 361 therein. (c) Schmid, G.; Maihack, V.; Lantermann, F.; Peschel, S. *J. Chem. Soc., Dalton Trans.* **1996**, 589. (d) Henglein, A.; Ershov, B. G.; Malow, M. *J. Phys. Chem.* **1995**, *99*, 14129. (e) Bönnemann, H.; Brijoux, W.; Brinkmann, R.; Fretzen, R.; Joussen, T.; Koppler, R.; Korall, B.; Neiteler, P.; Richter, J. *J. Mol. Catal.* **1994**, *86*, 129. (f) Schmid, G.; Harms, M.; Malm, J.-O.; Bovin, J.-O.; van Ruitenbeck, J.; Zandbergen, H. W.; Fu, W. T. *J. Am. Chem. Soc.* **1993**, *115*, 2046. (g) Lee, T. R.; Whitesides, G. M. *Acc. Chem. Res.* **1992**, *25*, 266−272. (h) Toshima, N.; Takahashi, T. *Bull. Chem. Soc. Jpn.* **1992**, *65*, 400. (i) Lee, T. R.; Whitesides, G. M. *Catal. Lett.* **1991**, *9*, 461−472. (j) Lee, T. R.; Whitesides, G. M. *J. Am. Chem. Soc.* **1991**, *113*, 368−369. (k) Lee, T. R.; Laibinis, P. E.; Folkers, J. P.; Whitesides, G. M. *Pure Appl. Chem.* **1991**, *63*, 821−828. (l) Vargaftik, M. N.; Zargorodnikov, V. P.; Stolarov, I. P.; Moiseev, I. I.; Kochubey, D. I.; Likholobov, V. A.; Chuvilin, A. L.; Zamaraev, K. I. *J. Mol. Catal.* **1989**, *53*, 315−348. (m) Schmid, G.; Lehnert, A. *Angew. Chem., Int. Ed. Engl.* **1989**, *28*, 780−781. (n) Schmid, G.; Morun, B.; Malm, J.-O. *Angew. Chem., Int. Ed. Engl.* **1989**, *28*, 778. (o) Meguro, K.; Torizuka, M.; Esumi, K. *Bull. Chem. Soc. Jpn.* **1988**, *61*, 341. (p) Harrison, J. B.; Berkheiser, V. E.; Erdos, G. W. *J. Catal.* **1988**, *112*, 126. (q) Boutonnet, M.; Kizling, J.; Stenius, P.; Maire, G. *Colloids Surf.* **1982**, *5*, 209.

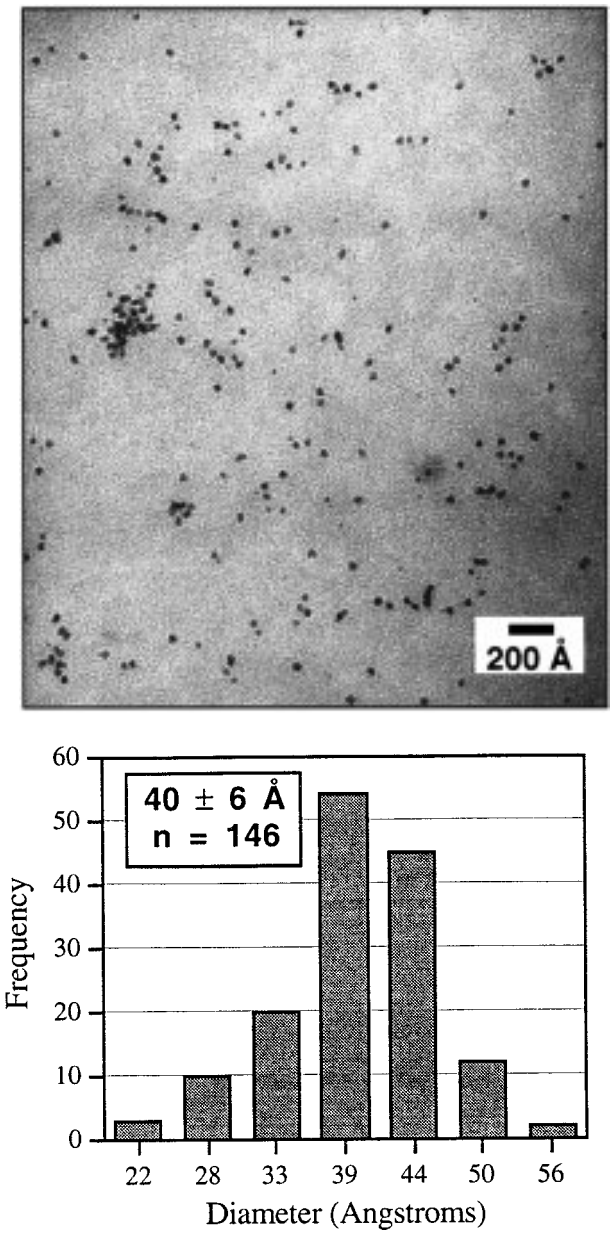

Figure 3. TEM image (300K magnification) and associated particle size histogram ($n = 146$ particles counted) of isolated, near-monodisperse 40 ± 6 Å Rh(0) nanoclusters grown by the reduction of 0.79 mM **2** in acetone under chemical-reaction-rate-limiting (i.e., *non*-MTL) conditions (3 °C, 49 ± 1 psig H_2). The reaction rate under these conditions is independent of stirring rate and is linearly dependent upon [**2**] (see Figure L in the Supporting Information), evidence demonstrating that these conditions are non-MTL. The sample was harvested after 100% conversion of **2** into nanoclusters (i.e., after GLC analysis showed that 1.0 equiv of cyclooctane had evolved from **2**).

manner that disfavors hydrogen MTL control, but favors chemical-reaction-rate control, of the synthesis.

Formation and Characterization of Near-Monodisperse 40 ± 6 Å Rh(0) Nanoclusters under Non-MTL Conditions. Figure 3 shows the results obtained following a change in three key reaction variables in a way to help avoid hydrogen mass-transfer limitations: higher H_2 pressure (which increases H_2 solubility), lower temperature (which slows subsequent reaction chemistry that uses H_2),[12] and lower precatalyst concentration (which also slows subsequent solution chemistry that uses H_2). These changes resulted in the formation of near-monodisperse, 40 ± 6 Å $Rh(0)_{\sim 1500}$ to $Rh(0)_{\sim 3700}$ nanoclusters.[13] Additional experiments, reported below, confirm that these pressure, temperature, and precatalyst concentration conditions avoid any problems with hydrogen mass transfer. In short, the two key results here are (i) the strong evidence for MTL effects in these particular nanocluster syntheses under H_2 and (ii) the design of conditions for the successful synthesis of near-monodisperse Rh(0) nanoclusters.

Characterization of the Rh(0) nanoclusters was accomplished by TEM and EDX analysis. TEM images (Figure 3) show nonaggregated, near-monodisperse, 40 ± 6 Å spherical nanoclusters.[14] [TEM images at lower (100 K) and higher (400 K) magnifications of these clusters are shown in Figure A of the Supporting Information.] EDX analysis on this sample detects O, Nb, and W, as well as Rh, confirming that the nanocluster stabilizing[6a,8,9] polyoxoanion, $P_2W_{15}Nb_3O_{62}^{9-}$, is also present.[15]

As in the formation of near-monodisperse 20 ± 3 Å $Ir(0)_{\sim 300}$ nanoclusters,[8a,b] analytical curve-fitting of the hydrogen pressure vs time data[16] obtained during this reaction can be accomplished if one incorporates our previously elucidated[8] nucleation ($A \rightarrow B$), and then autocatalytic, surface-growth ($A + B \rightarrow 2B$), steps, Supporting Information, Figure B. This is strong evidence that near-monodisperse Rh(0) nanoclusters—just like their near-monodisperse $Ir(0)_{\sim 300}$ analogues—form via the previously deduced mechanism involving these two steps, Scheme 1.[8a]

Formation of Polydisperse Ir Nanoclusters under Deliberately Induced Hydrogen MTL Conditions. An important question to answer is the following: If we deliberately pick conditions which *disfavor* hydrogen mass transfer, specifically the extreme conditions of a nonstirred solution, can we cause the formation of amorphous, bulk Ir(0) metal? That is, can we induce the opposite result compared to the synthesis of the near-monodisperse $Ir(0)_{\sim 300}$ nanoclusters shown in Figure 1, obtained at stirring rates of ≥400 rpm? Figure 4 shows the results of a deliberate and successful attempt to induce MTL conditions in the case of the Ir(0) nanoclusters. This result provides good evidence for the broader applicability of H_2 MTL effects in transition metal nanocluster syntheses.

Additional Evidence for a Hydrogen MTL Regime. (I) Establishment of a Stirring Rate Dependence on the Reac-

(12) The H_2 concentration in neat acetone at 49 psig H_2 and 3 °C is 1.5×10^{-2} M, unchanged (within experimental error) from its concentration at 40 psig H_2 and 22 °C. Thus, increasing the H_2 pressure from 40 to 49 psig H_2 compensates for the decrease in H_2 solubility at lower temperatures, and suggests that slower reaction chemistry—and not the dissolved H_2 concentration—is responsible for the change in particle dispersity in this case. H_2 solubilities were calculated by using both Ostwald coefficients (*The Matheson Unabridged Gas Book; Hydrogen*; Matheson: East Rutherford, NJ, 1974) and mole fraction data (*Solubility Data Series: Hydrogen and Deuterium*; Pergamon Press: New York, 1981; p 224).

(13) The 40 ± 6 Å or 34 to 46 Å nanoclusters yield approximate metal content numbers of $Rh_{\sim 1500}$ to $Rh_{\sim 3700}$, calculated as before[6a] with the equation $N = N_o rV/MW$ where $N_o = 6.02 \times 10^{23}$ atoms/mol, $r = 12.41$ g/cm^3, $V = 4/3\pi(D/2)^3$, and MW = 102.9 g/mol. That is, 34 and 46 Å rhodium particles contain ≈1500 and 3700 metal atoms, respectively, while a perfect, spherical 40 Å rhodium particle contains ≈2430 metal atoms. While the values of 1500 and 3700 metal atom particles are close to the number of atoms predicted in so-called "magic number" clusters (at 1415 and 3871), the number of atoms in a 40 Å rhodium particle (≈2430) falls between the two magic number values of 2057 and 2869.[8a] Hence, we have avoided in this instance the approximate nomenclature "$Rh(0)_{\sim 2400}$" as it is potentially misleading.[6c]

(14) Interestingly, the 40 Å diameter of our rhodium nanoclusters is close to those for Rh synthesized elsewhere with alcohol reductants, Os (~<10 Å) < Ir (14−30 Å) < Pt (27 Å) < Rh (~40 Å) < Pd (53 Å); see: Hirai, H.; Toshima, N. *J. Macromol. Sci. Chem.* **1979**, *A13(6)*, 727.

(15) As expected, peaks for Na, Cr, and Cu are also seen. Na is present as a countercation (from the precursor **2**) whereas the Cr peak comes from the specimen holder and the Cu peak comes from the copper grid. Being below the limit of detection, peaks for C and N are not seen but must also be present given that $[(n\text{-}C_4H_9)_4N]^+$ is present in the precursor **2**.

(16) Lyon, D. K.; Finke, R. G. *Inorg. Chem.* **1990**, *29*, 1787.

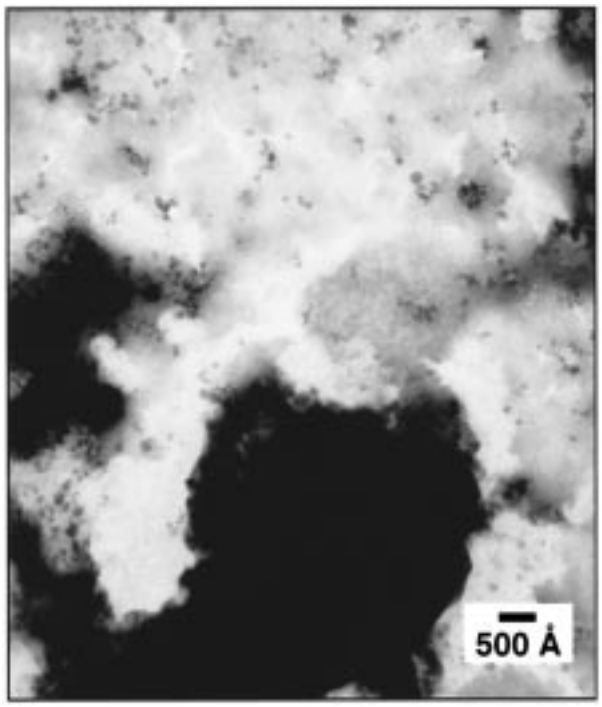

Figure 4. TEM image (at lower, 50K magnification) of the isolated, predominately bulk Ir(0) metal iridium product formed in an unstirred solution. (A small number of irregular and aggregated clusters are also seen at higher magnifications, Supporting Information, Figure K.)

tion Rate and on the Nanocluster Morphology. One classic simple, but convincing, piece of evidence for the presence of a gas-to-solution MTL regime is a demonstration of a stirring-speed dependence to the observed reaction rate.[17] Typically, such a stirring-rate dependence can then be changed to stirring-rate *independence* at higher stirring speeds, corresponding to a change to a non-MTL, chemical-reaction-rate-limiting, regime.

This predicted stirring-rate dependence is exactly what is seen in the present case, Figure 5, which shows the cyclohexene hydrogenation rate as a function of stirring rate for both iridium (Figure 5A) and rhodium (Figure 5B) nanoclusters. The first two points in Figure 5A (iridium) correspond to the limits of hydrogen MTL (point 1; 0 rpm) and non-MTL (point 2; vortex stirring at 400 ± 40 rpm) conditions. Additionally, point 3 (far right; 1300 ± 130 rpm) is well into the non-MTL regime. The only additional, confirming data that is needed here is TEM evidence for the shape and polydispersity or near-monodispersity of the nanoclusters grown at each point on this curve. In fact, point 1 in Figure 5A (0 rpm) represents the exact same sample used for the TEM image (amorphous bulk Ir(0) metal) shown in Figure 4. (A few nanoclusters are present, but they are mostly aggregated.) In contrast to this, TEM images of the Ir nanoclusters grown and isolated at points 2 and 3 *show well-defined and unaggregated, near-monodisperse individual clusters* analogous to the ones shown in Figure 1.

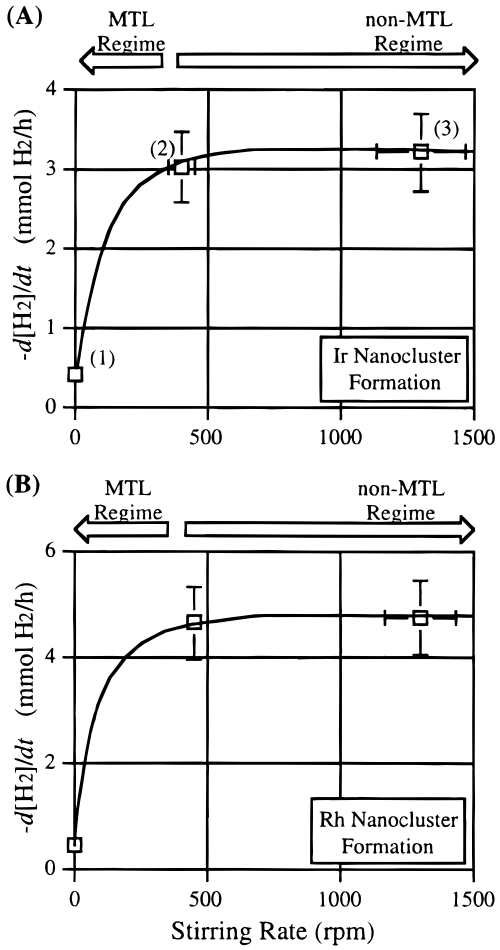

Figure 5. Hydrogenation rate of cyclohexene as a function of stirring rate under chemical-reaction-rate-limiting, non-MTL conditions beginning with **1** and showing saturation kinetics (A; 1.2 mM **1**, 40 ± 1 psig H_2, 22 °C) and **2** (B; 1.2 mM **2**, 49 ± 1 psig H_2, 3 °C). Rates in A: 0 rpm, 0.4 mmol H_2/h; 400 ± 40 rpm, 3.0 mmol H_2/h; 1300 ± 130 rpm, 3.3 mmol H_2/h. Rates in B: 0 rpm, 0.4 mmol H_2/h; 450 ± 45 rpm, 4.6 mmol H_2/h; 1300 ± 130 rpm, 4.7 mmol H_2/h. TEM images of the isolated reaction products at 400 and 1300 rpm (right-most two points; chemical-reaction-rate-limiting regime) show mostly individual, nonaggregated, near-monodisperse iridium nanoclusters (see Figure 1), whereas TEM images of the major product isolated at 0 rpm stirring [mass-transfer-limiting regime] exhibit amorphous, aggregated Ir(0) metal (shown at 50K magnification in Figure 4 in the text and at 200K magnification in Figure K of the Supporting Information).

The stirring rate curves, Figure 5, plus the TEM evidence for the drastic difference in cluster morphology of these two examples provide additional evidence for hydrogen gas-to-solution MTL effects in the present nanocluster syntheses under hydrogen.

(II) Demonstration of Catalyst Dependent and Nondependent Kinetic Regimes. A second, classic piece of evidence for a mass-transfer-limiting kinetic regime[17] is a demonstration that one can go from a catalyst-dependent (reaction-rate limiting) kinetic regime (e.g., typically a first-order dependence on catalyst) to a regime zero order in catalyst (the MTL regime). Figure 6, the rhodium nanocluster growth rate as a function of [**2**] and hydrogen pressure (40 or 49 psig H_2) at 22 °C, exhibits just such a phenomenon. At 40 psig H_2, this growth rate reaches a saturation point above ca. 1.0 mM [**2**], indicating that the

(17) A few lead references to the more extensive literature of mass-transfer-limited reactions: (a) Roberts, G. W. In *Catalysis in Organic Synthesis*; Rylander, P. N., Ed.; Conference on Catalysis in Organic Syntheses; Academic Press: New York, 1976; pp 1−48. (b) Hobbs, C. C.; Drew, E. H.; Van't Hof, H. A.; Mesich, F. G.; Onore, M. J. *Ind. Eng. Chem. Prod. Res. Dev.* **1972**, *11*, 220. (c) Gogate, M.; Lee, S. *Fuel Sci. Technol.* **1994**, *12*, 35−50. (d) Mathieu, C.; Dietrich, E.; Delmas, H.; Jenck, J. *Chem. Eng. Sci.* **1992**, *47*, 2289. (e) Notheisz, F.; Zsigmond, Á.; Bartók, M.; Szegletes, Z.; Smith, G. V. *App. Catal. A: General* **1994**, *120*, 105−114 and refs 1−9 therein. Note that the key test for gas−liquid MTL typically involves showing whether the rate law contains a first-order, [catalyst]^1 rate dependence. The equation cited therein of $-d[H_2]/dt = k_r k_m \cdot x/[k_r \cdot x + k_m]$ is useful in this regard (k_r = the chemical reaction-rate-limiting rate constant; k_m = the mass-transfer-limiting kinetic coefficient). (f) See also references b−f herein. (g) H_2 MTL effects on enantioselectivity in asymmetric catalysis: Sun, Y.; Landau, R. N.; Wang, J.; LeBlond, C.; Blackmond, D. G. *J. Am. Chem. Soc.* **1996**, *118*, 1348−1353.

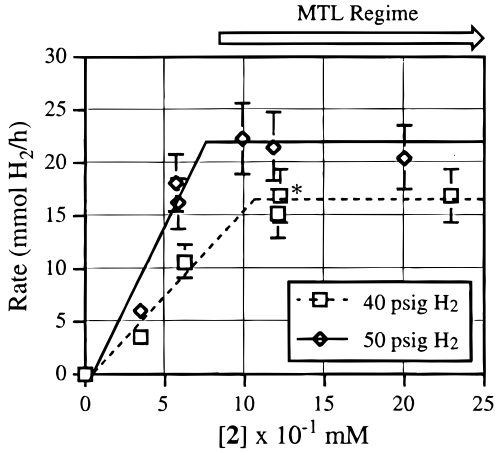

Figure 6. Hydrogenation rate of cyclohexene as a function of [**2**] at 22 °C and stirring ≥750 rpm at both 40 ± 1 psig H_2 (squares; dotted line) and 49 ± 1 psig H_2 (diamonds; solid line). The rate is initially dependent upon [**2**] and hydrogen pressure, but then shows saturation kinetics in both [**2**] and hydrogen. At saturation, the reaction is under hydrogen MTL conditions. The rhodium nanoclusters isolated at the point indicated by the asterisk (*) on the plot are polydisperse, as the TEM image in Figure 2 demonstrates.

reaction is operating under hydrogen MTL conditions at this (and higher) precatalyst concentration. Indeed, the irregular, polydisperse rhodium nanoclusters shown in Figure 2 were grown and isolated under the conditions labeled with the asterisk (∗) in Figure 6, conditions that are within the zero order in catalyst—and hence MTL—regime. Rather clearly, then, these stirring rate, TEM, and catalyst dependent vs nondependent kinetic data demonstrate that hydrogen gas-to-solution MTL conditions can drastically affect nanocluster particle size and morphology.

TEM Evidence Ruling Out Mechanisms That Involve a Time-Dependent Interconversion between Near-Monodisperse and Polydisperse Nanoclusters. Three key pieces of evidence presented so far are the following: (i) that hydrogen MTL conditions can directly affect particle size and morphology, (ii) that iridium and rhodium nanoclusters grown under reaction-rate-limiting conditions are near-monodisperse, and (iii) that iridium and rhodium nanoclusters grown under hydrogen MTL conditions are polydisperse. This evidence, plus the literature evidence for the generality of diffusive agglomeration of nanoclusters,[5,18] is fully consistent with two *parallel, kinetically competing* reactions[19] leading to near-monodisperse vs polydisperse nanoclusters, Scheme 2.[20]

Note that one prediction of this scheme is that the ratio of polydisperse to monodisperse nanoclusters should increase with time *if* the reaction happened to be in a regime where both processes are kinetically competitive. Alternatively, a second prediction is that if the reaction is in the *non*-MTL regime (i.e., where generally only autocatalytic growth and no diffusive agglomeration has been seen[8a]), then only monodisperse nanoclusters are predicted throughout the whole reaction. TEM at both short (≤20%) and near-completion (≥95%) reaction times was used to rule out alternative mechanisms involving an interconversion between poly- and mono-disperse nanoclusters. This TEM experiment was carried out by first harvesting both Ir(0) and Rh(0) nanoclusters (seven samples total) at times corresponding to ≤20% M(0) formation and ≥95% M(0) formation. The cyclooctane product yield accompanying the conversion of the 1,5-COD in the precatalysts **1** and **2**, eq 1 (a direct monitor of the M(0) formation[8a]), was also determined by GLC (as detailed in the Experimental Section). The experiment and the cyclooctane evolution results are shown in Figure 7, and Table 1 summarizes the degrees of dispersity determined by TEM for the seven samples.

Scheme 2. Two Precedented, Parallel Nanocluster Growth Pathways: Autocatalysis[8a] (top pathway) Leading to *Near-Monodisperse* Nanoclusters, and Diffusive Agglomerative Growth[18] (bottom pathway) Leading to *Polydisperse* Nanoclusters

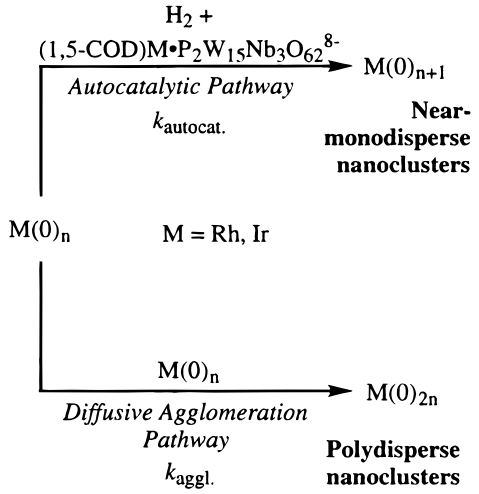

The key results are that the resulting nanoclusters have the same dispersity, regardless of whether they are isolated at ≈100% or at ≤20% precatalyst conversions and regardless if they are Rh or Ir nanoclusters, so long as the conditions were MTL or non-MTL throughout the synthesis. For example, when Rh(0) nanoclusters grown under MTL conditions are isolated at ≤20% conversion of the precatalyst **2**, the resulting distribution of diameters is broad (ranging from ca. 20 to 80 Å), and *bimodal* [21] (centering around 37 and 48 Å) and thus polydisperse, Figure C, Supporting Information. However, when the Rh nanocluster synthesis is carried out under reaction-rate limiting, *non*-MTL conditions, TEM[22] shows that the Rh(0) nanoclusters are near-monodisperse, with an average diameter

(18) Lin, M. Y.; Lindsay, H. M.; Weitz, D. A.; Ball R. C.; Klein, R.; Meakin, P. Universality in Colloid Aggregation *Nature* **1989**, *339*, 360. Note that by "universality" these authors are referring to the literature of fractals and, hence, mean "independent of the details of the particular system" or "independent of the specific details of how the particular particles are formed". (b) For a review titled Fractal Aggregates, see Meakin, P. *Adv. Colloid Interface Sci.* **1988**, *28*, 249, which covers many of the proposed mechanisms, computer simulations, and some of the experimental evidence on colloid aggregation phenomenon.

(19) (a) Moore, J. W.; Pearson, R. G. *Kinetics and Mechanism*, 3rd ed.; John Wiley & Sons: New York, 1981; pp 299−304. (b) Espenson, J. H. *Chemical Kinetics and Reaction Mechanisms*; McGraw-Hill: New York, 1981; pp 57−59.

(20) (a) We note that a *Nature* paper has appeared offering evidence that aggregation is "universal" in the fractal sense. Also noteworthy here is that we previously cited our one, preliminary piece of evidence for a parallel step of diffusive agglomeration (Step V, Scheme 1) in competition with autocatalytic nanocluster growth (Step IV, Scheme 1), specifically our initial observation of nanoclusters that were "less spherical [in] shape" when grown under lower H_2 pressure conditions in iridium nanocluster syntheses.[6a] But, as we noted previously, the proposed agglomeration step was, at that time, "the only step in the minimum mechanism in [Scheme 2 of that report] that is on less solid grounds".

(21) (a) A bimodal distribution under MTL conditions, and at ≤20% conversion, means that nucleation is initiated at two, rather different times, just as expected when H_2 is not uniformly present throughout the solution under MTL conditions. However, given that isolation of rhodium nanoclusters at *100% conversion* under identical conditions yields smaller (40 ± 14 Å), polydisperse nanoclusters (as compared to the bimodal distribution centered about 37 and 48 Å obtained at ≤20% conversion), this explanation requires that the nanoclusters *decrease* in size and become closer to unimodal at some later time through, presumably, Ostwald ripening processes.

Table 1. Iridium and Rhodium Nanocluster Dispersities as a Function of Reaction Conditions (non-MTL vs MTL) and Nanocluster Isolation Times[a]

	iridium		rhodium	
	≤20% conversion	≥95% conversion	≤20% conversion	≥95% conversion
non-MTL conditions	near-monodisperse (20 ± 3 Å)	near-monodisperse (20 ± 3 Å)	near-monodisperse (34 ± 5 Å)	near-monodisperse (40 ± 6 Å)
MTL conditions		bulk Ir(0) metal	polydisperse; bimodal	polydisperse (40 ± 14 Å)

[a] The data show that, regardless of their individual isolation times, nanoclusters grown under *non*-MTL conditions are *near-monodisperse* while nanoclusters grown under MTL conditions are *polydisperse*. A statistical analysis for bimodality was performed on particle size histograms which appeared to be bimodal (i.e., the ≤20% conversion Rh example, Supporting Information, Figure C).

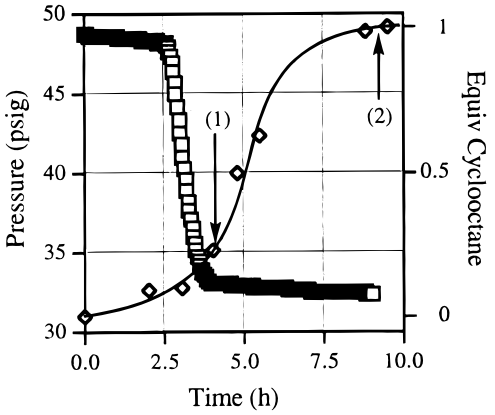

Figure 7. Co-plot of hydrogen pressure (squares; left axis) and cyclooctane production by GLC (diamonds, right axis: 0.09 equiv, 2.0 h; 0.10 equiv, 3.0 h; 0.23 equiv, 4.0 h; 0.50 equiv, 4.75 h; 0.63 equiv, 5.5 h; 0.98 equiv, 8.75 h; 1.0 equiv 9.5 h) versus time in the concomitant hydrogenation of cyclohexene and formation of near-monodisperse Rh(0) nanoclusters. (Conditions: 1.2 mM **2**, 1.65 M cyclohexene, 49 ± 1 psig H_2, 3 °C.) A ca. 2.5 h induction period is seen prior to the linear H_2 pressure loss, due to cyclohexene hydrogenation. The hydrogenation rate, $-d[H_2]/dt$, may be reliably calculated from the slope of the linear portion of the line.[8a] Point 1 shows the first time at which the nanoclusters were isolated (≤0.2 equiv cyclooctane produced) whereas point 2 shows the last time at which the nanoclusters were isolated (≥0.95 equiv cyclooctane produced).

of 34 ± 5 Å (Supporting Information, Figure D). These results rule out mechanisms that involve a time-dependent interconversion between mono- and poly-disperse nanoclusters; the results are, however, fully consistent with and supportive of the anticipated parallel growth pathways mechanism shown in Scheme 2.

Note that, under H_2 MTL conditions, one might expect nucleation to occur intermittently, thereby leading to polydisperse nanoclusters, if not to bimodal distributions. Hence, the observation of a statistically significant bimodal distribution of polydisperse nanoclusters (Figure C, Supporting Information) is good evidence for H_2 MTL effects on the *nucleation* step as well as on the subsequent competing autocatalytic surface growth, vs diffusive agglomeration, steps.

Control Experiment Demonstrating the Catalytic Activity of the *Isolated* Rh(0) Nanoclusters for Cyclohexene Hydrogenation. To demonstrate that the Rh(0) nanoclusters exhibit catalytic activity once isolated as a solid and redispersed in the presence of fresh cyclohexene, a catalytic cyclohexene hydrogenation reaction was performed beginning with ca. 2.5 mg of *isolated* Rh(0) nanoclusters dissolved in 2.5 mL of acetone and 0.5 mL of cyclohexene. The results show that the olefin hydrogenation reaction proceeds, as expected, without an induction period.[23] Indeed, we have found, and will report elsewhere,[24] conditions under which polyoxoanion-stabilized Rh(0) nanoclusters generated from **2** exhibit ≥150 000 total turnovers of cyclohexene hydrogenation.

Summary and Conclusions

The highlights of the present work can be summarized as follows:

(1) Hydrogen gas-to-solution MTL has been recognized as a factor that must be controlled in the synthesis of transition metal nanoclusters under H_2. This is especially true for the more catalytically active second-row transition metals such as Rh, or if the nanoclusters are formed in the presence of reducible substrates such as olefins. Since H_2 is one of the most common reducing agents for the synthesis of nanoclusters, this finding should be of broader significance and impact.

(2) Several lines of evidence [stirring rate, catalyst dependent or nondependent kinetic regimes, and TEM evidence, including a statistical analysis for bimodal distributions] were obtained for the existence of hydrogen MTL and non-MTL kinetic regimes, depending upon the exact conditions. These lines of evidence support a mechanism with two parallel, competing, nanocluster growth steps: autocatalytic surface growth, leading to near-monodisperse nanoclusters, and diffusive agglomeration, leading to polydisperse nanoclusters. Hydrogen MTL effects also negatively influence the nanocluster nucleation process, leading to bimodal distributions of nanoclusters.

(3) The above mechanistic insights allowed, in turn, the design of conditions leading to the synthesis of the desired, near-monodisperse, 40 ± 6 Å Rh(0) nanoclusters. These Rh(0) nanoclusters are of interest as only the second example of polyoxoanion-stabilized transition metal nanoclusters.

The availability, now, of both Rh(0) and Ir(0) polyoxoanion- and Bu_4N^+-stabilized nanoclusters is by no means trivial, since these nanoclusters are unusual among known transition metal nanoclusters in that they undergo extensive catalytic turnovers *in solution*, without the need for additional stabilization provided by either polymer protectants or by affixing them to solid supports.[2b] In future publications we will report on the scale-

(22) Sometimes TEM images of nanoclusters isolated at early, incomplete, or later reaction times show nanoclusters somewhat *clumped* together rather than completely and individually dispersed, even though a closer examination of the nanoclusters at higher magnification reveals that individual nanoclusters themselves are not fused. This seems to be an artifact of the deposition/TEM visualization process, so that one must be careful to distinguish individual but "*clumped*" particles from *fused*, and thus truly *agglomerated*, particles. This is perhaps why some investigators will sonicate or otherwise redisperse their particles prior to their TEM visualization, but we chose to not do this to avoid introducing any new artifacts that such a process might include. We note here that fractal aggregate type "clumps" are the expected result of agglomeration, for example Figure I of the Supporting Information, which looks distinctly fractal-like.

(23) Aiken, J. D., III; Finke, R. G. Polyoxoanion- and Tetrabutylammonium-Stabilized Near-Monodisperse, 40 ± 6 Å $Rh(0)_{\sim 1500}$ to $Rh(0)_{\sim 3700}$ Nanoclusters: Synthesis, Characterization and Hydrogenation Catalysis, manuscript in preparation.

(24) Aiken, J. D., III; Finke, R. G. Polyoxoanion- and Tetrabutylammonium-Stabilized Transition Metal Nanoclusters: Unprecedented Catalytic Lifetime in Solution. Manuscript in preparation.

up, isolation details, catalytic reactions, and the other properties of the polyoxoanion- and Bu_4N^+-stabilized Rh(0) nanoclusters.[23]

Experimental Section

Materials. Cyclohexene (Aldrich, 99+%, stabilized with 0.01% 2,6-di-*tert*-butyl-4-methylphenol) was distilled from Na under argon immediately prior to use (≥99% purity by GLC) and stored in a Vacuum Atmospheres drybox. Acetone (Burdick and Jackson, 0.26% H_2O) was transferred into the drybox and purged for ≥30 min with nitrogen using a glass bubbler. The source, purity, and water content of the acetone are known to be crucial to obtaining reproducible kinetic rates.[9] Toluene (anhydrous, 99.8%, packed under N_2, Aldrich) was degassed via 3 freeze−pump−thaw cycles and stored in the drybox. Hydrogen gas (General Air, 99.5%) used on the hydrogenation apparatus, vide infra, was prepurified by passage through a moisture trap (Scott Specialty Gases, Baxter Scientific), an oxygen trap (R&D Separations type OT3, Baxter Scientific), and an indicating oxygen trap (R&D Separations, Hewlett-Packard).

The polyoxoanion, $[(n\text{-}C_4H_9)_4N]_9P_2W_{15}Nb_3O_{62}$, used in the synthesis of **1** and **2**, was synthesized according to our more recent procedure.[7a] The air-sensitive polyoxoanion-supported organometallic precatalysts $[(n\text{-}C_4H_9)_4N]_5Na_3[(1,5\text{-COD})Ir{\cdot}P_2W_{15}Nb_3O_{62}]$, **1**, and $[(n\text{-}C_4H_9)_4N]_5Na_3[(1,5\text{-COD})Rh{\cdot}P_2W_{15}Nb_3O_{62}]$, **2**, were synthesized and characterized as previously reported[25] and stored in a drybox. The precatalyst **2** used for the data reported herein was a batch that exhibited the highest catalytic activity observed, $-d[H_2]/dt = 4.7$ mmol H_2/h at 49 psig H_2 and 3 °C. This particular batch of **2** was found to contain 0.20%, or 0.14 equiv, Br^- by elemental analysis. However, as detailed in the Supporting Information, control experiments show that this trace amount of Br^- has a negligible effect on the observed rates. (We do, however, recommend that one thoroughly wash the polyoxoanion complexes as previously detailed,[7a] thereby removing any trace amounts of remaining Br^-.)

Analytical Procedures. Unless otherwise reported all reaction solutions were prepared under oxygen- and moisture-free conditions with a Vacuum Atmospheres drybox (<1 ppm O_2 as continuously monitored by a Vacuum Atmospheres O_2-level monitor). Stirring rates were determined in revolutions per minute (rpm) with a Pocket-Tach 100 (Monarch Instrument).

Specimens were examined by transmission electron microscopy (TEM) either at CSU, using a JEOL TEM 2000 EX-II, or at the University of Oregon, using a Philips CM-12 with a 70 μm lens, the latter as previously described in detail.[6] Both microscopes were operated at an accelerating voltage of 100 keV. Samples examined by TEM at CSU were prepared with type A (300 mesh) Formvar and carbon coated copper grids (supplier, Ted Pella). Grids were gently suspended in chloroform for about 30 s immediately prior to use to remove the Formvar coating and to expose a fresh carbon surface. One drop of the nanocluster solution (at a concentration of ca. 1 mg/mL, in either acetone or acetonitrile, vide infra) was placed on the carbon-coated grid with a gas-tight syringe and allowed to air-dry. Samples were examined at magnifications between 100 and 400K, and in at least three different places on the sample grid to ensure that the images seen were representative of the sample as a whole. Reported magnifications are those of the original negative. Particle-size distributions were determined once the original negative had been digitally scanned into Adobe Photoshop and expanded to >20 in. × 25 in. for easier size measurement and resolution. Previously reported control experiments[6a] show (i) that the *iridium* nanocluster samples are not perturbed by changing either the electron beam accelerating voltage (40 or 100 keV) or by varying sample exposure times under the beam (seconds vs minutes) and (ii) that the iridium precursor **1** does not form nanoclusters under the TEM beam.[6a] A repeat herein of this latter control experiment, that is, using a solution of the *rhodium*-containing nanocluster precursor complex **2**, shows that it, too, does not form nanoclusters under TEM conditions which were identical to those used to examine the Rh(0) nanoclusters (Supporting Information, Figure E).

Nanocluster samples were analyzed by energy-dispersive X-ray analysis (EDX) on the JEOL TEM with a Kevex Super 8000, running Quantex Version 6.0, coupled to a Quantum thin window detector (mylar window; 30 mm^2 detector area with a resolution of 116 eV at 1.49 keV). Electron beam spot sizes (typically between instrument setting of 2 and 5) were adjusted so that events occurred with a deadtime of ≤50% at between 1000 and 2000 counts/s. The instrument was calibrated to the K lines of Al and Cu; peak assignments are based on emission energy and peak intensity.

Gas−liquid chromatography (GLC) was performed on a Hewlett-Packard 5890 Series II GC with a FID detector equipped with a 30 m (0.25 mm i.d.) Econo-cap Carbowax column (Alltech) and coupled to a Hewlett-Packard 3395 integrator. Parameters were as follows: initial temperature, 50 °C; initial time, 3 min; ramp, 10 °C/min; final temperature, 160 °C; final time, 16 min; injector port temperature, 180 °C; detector temperature, 200 °C; injection volume, 4 μL.

Hydrogenation Experiments ("Standard Conditions") and Calculation of Reaction Rates. Hydrogenation reactions were performed using our previously described pressurized hydrogenation apparatus[9] (Supporting Information, Figure F), except that it was equipped with an improved Pyrex water-jacketed reaction flask (200 mL; supplier, Andrews Glass Company). All reaction mixtures were prepared in a nitrogen-filled drybox. In each experiment, the precursors **1** or **2** were weighed into a 1 dram vial and dissolved in 2.5 mL of acetone (added via a 10 mL gas-tight syringe) to yield a clear, bright-yellow solution. Cyclohexene (0.5 mL, 1.65 M) was added and the resultant clear, homogeneous solution was transferred via polyethylene pipet into a fresh 22 × 175 mm borosilicate culture tube containing a 5/16 in. × 5/8 in Teflon-coated magnetic stir bar. The culture tube was then sealed inside of a Fischer−Porter pressure bottle that is part of the hydrogenation apparatus (Figure F, Supporting Information); the Fischer−Porter bottle was brought outside of the drybox, placed inside a constant temperature circulating water bath (Neslab Escal, ±0.1 °C), and attached to the hydrogenation line via Swagelock TFE-sealed Quick-Connects. (Before attachment of the Fischer−Porter bottle to the hydrogenation line, the line itself was evacuated for at least 1 h to remove any trace oxygen and water present, and then refilled with purified hydrogen.) The Fischer−Porter bottle was then purged 15 times with hydrogen (15 s per purge, with stirring) and stirred vigorously for 2 min, and then $t = 0$ was set. Hydrogen pressure in the Fischer−Porter bottle was then monitored with an Omega Model PX621 pressure transducer attached to an IBM PC via an Omega WB35 A/D converter. Pressure vs time data were processed with Microsoft Excel.

Reaction rates were calculated from the rate of hydrogen pressure loss ($-d[H_2]/dt$, expressed in mmol H_2/h) as determined by the slope of the linear portion of the H_2 uptake curve, an example of which is shown in Figure 7. As demonstrated elsewhere,[8a] this slope correlates linearly with the bimolecular rate constant k_2, obtained by quantitative curve-fitting of the hydrogen pressure vs time data to the appropriate nucleation plus autocatalytic growth kinetic expressions.[8a]

Nanocluster Sample Isolation and Preparation for TEM Analysis. The Fischer−Porter bottle containing the reaction solution was disconnected from the hydrogenation line via the Quick-Connects and taken back into the drybox, the hydrogen pressure was released, and the turbid nanocluster solution was poured into a 1 dram vial which was capped with a plastic snap-cap. The turbid solution was then allowed to stand undisturbed in the drybox for ≥10 h, after which time the nanoclusters had settled to form a black precipitate. The supernatant was carefully removed via a polyethylene pipet and discarded. While still in a drybox, the black nanocluster precipitate (now in ≤0.5 mL of solution) was then dried under vacuum overnight at room temperature to yield a black powder. A TEM sample was prepared by redissolving all of this black powder in 3 mL of fresh acetone or acetonitrile to yield a clear amber, homogeneous solution (no bulk metal was visible by the naked eye at any time). A drop of this solution was then dispersed on a chloroform-cleaned TEM grid.

(25) $(1,5\text{-COD})M{\cdot}P_2W_{15}Nb_3O_{62}^{8-}$: (a) Nomiya, K.; Pohl, M.; Mizuno, N.; Lyon, D. K.; Finke, R. G. In *Inorganic Syntheses*; Cowley, A. H., Ed.; John Wiley and Sons: New York, 1997; Vol. 31, pp 186−201. (b) Pohl, M.; Lyon, D. K.; Mizuno, N.; Nomiya, K.; Finke, R. G. *Inorg. Chem.* **1995**, *34*, 1413. (c) Pohl, M.; Finke, R. G. *Organometallics* **1993**, *12*, 1453−1457. (d) Finke, R. G.; Lyon, D. K.; Nomiya, K.; Sur, S.; Mizuno, N. *Inorg. Chem.* **1990**, *29*, 1784−1787.

Quantitative Curve-Fitting of Hydrogen Pressure *vs* Time Data. Curve-fitting of the hydrogen pressure (or, equivalently, cyclohexene concentration[8a]) vs time data was performed as previously described.[8a] Briefly, a nonlinear regression subroutine (RLIN), using a modified Levenberg−Macquard algorithm and available in the IMSL Statistical Library, was used (running on an IBM/AIX workstation). As a control, the curve-fitting program was first tested on a previously published data set[8a] and faithfully reproduced k_1 and k_2 values from that data set. Curve-fits of two rhodium nanocluster formation runs under non-MTL conditions are supplied as Figure B of the Supporting Information.

Statistical Analysis for Bimodality in Particle Size vs Frequency Histograms. A program was written in S-plus that utilizes a bootstrap databased simulation method[26] for determining the percent confidence of bimodality in particle size vs frequency distributions which contain more than one mode (i.e. Figure C of the Supporting Information). This was applied to particle size histograms which appeared to contain more than one mode. Full details are given in the Supporting Information.

Formation of *Polydisperse* Rh(0) Nanoclusters by Hydrogenation of Cyclohexene under Hydrogen Mass-Transfer-Limiting Conditions. A cyclohexene hydrogenation was performed under conditions identical to those previously reported (i.e., the Standard Conditions[6a,9]) *except* with the rhodium precursor **2**, $[(n\text{-}C_4H_9)_4N]_5Na_3[(1,5\text{-COD})Rh{\cdot}P_2W_{15}Nb_3O_{62}]$. A clear, bright-yellow solution of **2** (20.5 mg, 3.7×10^{-3} mmol) was made by dissolving the complex in 2.5 mL of acetone and 0.5 mL of cyclohexene. A Standard Conditions hydrogenation reaction was carried out as described above at 22 °C and with an initial pressure of 40 psig H_2 (3.7 atm). When the reaction was complete, the Fischer−Porter bottle was disconnected from the hydrogenation apparatus and transferred into the drybox and the hydrogen pressure was released. The rhodium nanoclusters were isolated as described in the Nanocluster Sample Isolation section and examined by TEM. The results are presented in Figure 2. A histogram of the observed 16 to 116 Å frequency vs particle diameter is shown in Figure G of the Supporting Information.

With the goal of elucidating the hydrogenation rate vs [**2**] dependence curve, eleven additional cyclohexene hydrogenation reactions at 22.0 ± 0.1 °C were performed at either 40 ± 1 or 49 ± 1 psig H_2 (two sets of experiments); the concentration of **2** was varied between 0.3 and 2.3 mM at each pressure. The results of this series of 12 experiments are summarized in Figure 6.

Formation of *Near-Monodisperse* 40 ± 6 Å Rh(0) Nanoclusters by Hydrogenation of Cyclohexene under Reaction-Rate-Limiting (*Non*-MTL) Conditions. The synthesis of near-monodisperse 40 ± 6 Å Rh(0) nanoclusters was carried out in the exact manner described above for the Standard Conditions *except* for the following changes designed to avoid hydrogen mass-transfer limitations: (a) the amount of the precatalyst **2** was lowered to 13.3 mg (2.4×10^{-3} mmol, 0.79 mM) to slow the reaction and to lower the demand for H_2; (b) the reaction temperature was reduced to 3.0 ± 0.1 °C to slow the reaction; and (c) the initial hydrogen pressure was increased to 49 ± 1 psig H_2. After complete conversion of the precursor **2** into nanoclusters (≥8 h; confirmed by the release of 1.0 equiv of cyclooctane by GLC, vide infra), the Fischer−Porter bottle containing the turbid, yellow-brown reaction solution was taken into the drybox and the remaining hydrogen pressure was released. The clusters were isolated as described above and then examined by TEM (Figure 3) and EDX (Supporting Information, Figure H). Two additional TEM images of this same sample at higher (400K) and lower (100K) magnifications are shown in Figure A of the Supporting Information.

GLC Determination of the Evolved Equivalents of Cyclooctane *vs* Time during Rh(0) Nanocluster Formation. Toluene (2 μL; as a GLC internal standard) was added with a 5 μL gas-tight syringe to a clear, bright-yellow solution of **2** (20.1 mg, 3.6×10^{-3} mmol, 1.2 mM) dissolved in 2.5 mL of acetone and 0.5 mL of cyclohexene. A hydrogenation reaction was then started by using an initial hydrogen pressure of 49 psig and at a temperature of 3 °C (non-MTL conditions). At prechosen times, the hydrogen pressure was released and aliquots (≤0.1 mL) of the reaction solution were drawn with an 18 in. needle attached to a gas-tight syringe that was inserted through the ball valve at the top of the Fischer−Porter bottle, Figure F, Supporting Information, all while under a continuous flow of H_2. Aliquots were removed only after the needle and syringe were purged thoroughly with H_2. Once the aliquot was taken, the Fischer−Porter bottle was purged an additional five times (15 s per purge) with hydrogen gas and resealed at 49 psig H_2. The production of cyclooctane vs time is summarized in Figure 7.

Hydrogenation of Cyclohexene Beginning with 1 and 2 as a Function of the Stirring Rate. The effect of stirring rate on nanocluster formation was measured in a series of otherwise Standard Conditions experiments at a constant precursor concentration (20.0 ± 2.0 mg, $3.6 \pm 0.3 \times 10^{-3}$ mmol, 1.2 ± 0.1 mM) by using both the iridium-containing precursor **1** (at 40 psig H_2 and 22 °C, non-MTL conditions) and the rhodium-containing precursor **2** (at 49 psig H_2 and 3 °C, non-MTL conditions). Hydrogenation rates vs stirring rate (rpm) beginning with **1** are summarized in Figure 5A. Hydrogenation rates vs stirring rate beginning with **2** are summarized in Figure 5B.

Mechanistic TEM Studies. Isolation and TEM Examination of Iridium and Rhodium Nanoclusters at ≤20% Reaction Times. To determine if the degree of polydispersity of the iridium and rhodium nanoclusters changed throughout the reaction under both MTL and non-MTL conditions, a series of nanoclusters were grown and isolated at ≤20% of their growth cycle (see point 1 in Figure 7, the point at which hydrogen consumption was complete) and examined by TEM for their degree of dispersity. In all experiments the initial precatalyst concentration was constant at 1.2 ± 0.1 mM. When cyclohexene hydrogenation was complete (point 1, Figure 7), the reaction was quenched by stopping the stirring, releasing the hydrogen pressure, and transferring the Fischer−Porter bottle and its turbid-yellow reaction solution back into the drybox. Next, the nanoclusters were isolated as detailed in the Nanocluster Sample Isolation section, then redissolved in 3 mL of CH_3CN for TEM analysis. The degree of dispersity in each case is shown in Table 1. The corresponding TEM images and particle size histograms are shown in the Supporting Information: Figure C, Rh, MTL conditions, 44 ± 11 Å, a bimodal distribution; Figure D, Rh, non-MTL, 34 ± 5 Å; Figure I, Ir, non-MTL, 20 ± 3 Å.

Investigation of the Origins of the 5-Fold Rh(0) Nanocluster Precursor-Batch-Dependent Variability in the Observed Catalytic Rates. Throughout the course of other work,[23] we found that 2 of 7 of the batches of Rh precursor **2** showed catalytic hydrogenation rates which were ca. 5-fold faster that the slowest batch under identical reaction conditions. (The two fastest batches of Rh(0) nanoclusters were used for the present studies of MTL effects, except for the control experiment below, since these studies were done first, before our other Rh(0) nanocluster work,[23] and since the early two batches of Rh(0) nanoclusters were the 5-fold faster ones.) However, within a batch of Rh precursor **2**, the rates were the reproducible 15−20% we have seen previously, even inter-batch, for the Ir precursor.[6a,8] As a source of this variability we considered trace oxygen,[27] trace Br^- (see the Supporting Information), or possibly trace water remaining in the hydrogenation apparatus itself. However, data presented herein and elsewhere demonstrated that this variability is *not* due to O_2, or Br^-, or the apparatus; hence, we conclude it is intrinsic to the precatalyst **2** itself (which is known to exist as ≥2 isomers[25b]), and thus most likely variability in the nanocluster nucleation (and possibly also growth) steps. Note, however, as the control experiment below demonstrates, this variability *does not* affect the general results obtained herein under MTL conditions. Hence, this variability as a function of the batch of precatalyst **2** is addressed in more detail elsewhere.[23]

Control Experiment Demonstrating That H_2 MTL Effects Are Found in the Slower Batch of Rh(0) Nanoclusters. As a control, an

(26) Efron, B.; Tibshirani, R. J. *An Introduction to the Bootstrap*; Monograph on Statistics and Applied Probability 57; Chapman & Hall: New York, 1993; pp 227−234.

(27) Structural studies or catalytic effects of oxygen in small metal particle systems: (a) Harada, M.; Asakura, K.; Ueki, Y.; Toshima, N. *J. Phys. Chem.* **1992**, *96*, 9730−9738. (b) Reetz, M. T.; Quaiser, S. A.; Winter, M.; Becker, J. A.; Schäfer, R.; Stimming, U.; Marmann, M.; Vogel, R.; Konno, T. *Angew. Chem., Int. Ed. Engl.* **1996**, *35*, 2092. (c) Kolb, W.; Quaiser, S.; Winter, M.; Reetz, M. T. *Chem. Mater.* **1996**, *8*, 1889−1894. (d) Rothe, J.; Pollmann, J.; Franke, R.; Hormes, J.; Bönnemann, H.; Brijoux, W.; Siepen, K.; Richter, J. *Fresenius J. Anal. Chem.* **1996**, *355*, 372−274. (e) See also p 371 of ref 1i.

experiment was done to show that Rh(0) nanoclusters, formed from a batch of **2** that gave the slowest observed cyclohexene hydrogenation catalytic rate ($-d[H_2]/dt = 1.0$ mmol H_2/h at 49 psig H_2 and 3 °C), still show MTL effects. Specifically, under nonstirred (0 rpm) reaction conditions, the results, Figure J, Supporting Information, show the presence of both aggregated Rh(0) metal and polydisperse and irregular shaped 35 ± 11 Å Rh(0) nanoclusters (ca. 31% polydispersity). This control experiment confirms that the general conclusions of this study—that is, the observation of H_2 MTL effects—are not dependent upon the particular batch of Rh(0) precursor **2** employed.

Acknowledgment. We wish to thank Dr. Eric Schabtach at the University of Oregon for obtaining the TEM image shown in Figure 2. We also thank Dr. John Chandler at the Colorado State University Electron Microscopy and Digital Imaging Center for helpful assistance with TEM images obtained at CSU and Prof. Phil Chapman and Mr. Shannon Ritter in the Statistics Department at CSU for performing the bimodal statistical analysis cited in the text. Financial support was provided by the Department of Energy, Chemical Sciences Division, Office of Basic Research, via grant DOE FG06-089ER13998.

Supporting Information Available: Figure A, two additional TEM images (at 100 and 400K magnifications) of the near-monodisperse Rh(0) nanocluster sample shown in Figure 3; Figure B, curve-fitting of the hydrogen pressure vs time data for the synthesis of rhodium nanoclusters grown under non-MTL conditions; Figure C, TEM image and associated histogram of polydisperse rhodium nanoclusters following isolation at ≤20% precursor conversion under MTL conditions; Figure D, TEM image and associated histogram of near-monodisperse rhodium nanocluster diameters following isolation at ≤20% precursor conversion under non-MTL conditions; Figure E, TEM image (at 300K magnification) of a solution of **2** showing that nanoclusters are not formed from **2** under TEM conditions; Figure F, detailed schematic of the hydrogenation apparatus used in the present study; Figure G, histogram of rhodium particle diameters corresponding to Figure 2; Figure H, EDX spectroscopy on the Rh(0) nanoclusters shown in Figure 2; Figure I, TEM image and associated histogram of near-monodisperse $Ir(0)_{\sim 300}$ nanocluster diameters following isolation at ≤20% precursor conversion under non-MTL conditions; Figure J, TEM and associated histogram of irregular shaped, polydisperse 35 ± 11 Å Rh(0) nanoclusters grown under MTL conditions (0 rpm stirring) for a slower batch of Rh(0) nanoclusters; Figure K, amplified TEM image (200K magnification) of bulk Ir(0) metal produced at 0 rpm stirring and shown at 50K magnification in Figure 4; Figure L, observation of, and explanation for, the non-hydrogen pressure dependence when under non-MTL conditions; statistical analysis for bimodality in particle size vs frequency histograms; control experiments describing the rate-enhancing effects of added tetrabutylammonium bromide on the observed catalytic hydrogenation activity beginning with **2** (15 pages, print/PDF). See any current masthead page for ordering information and Web access instructions.

JA9719485